Available online at www.sciencedirect.com
SCIENCE DIRECT®
International Journal of Multiphase Flow 31 (2005) 706–722
International Journal of Multiphase Flow
www.elsevier.com/locate/ijmulflow

Micro-fabricated electrolytic micro-bubblers

S. Lee [a], W. Sutomo [a], C. Liu [a], E. Loth [b,*]

[a] Department of Mechanical Engineering, University of Illinois at Urbana-Champaign, Urbana, IL 61801-2935, USA
[b] Department of Aerospace Engineering, University of Illinois at Urbana-Champaign, 306 Talbot Laboratory, 104 S. Wright Street, Urbana, IL 61801-2935, USA

Received 3 May 2004; received in revised form 2 February 2005

Abstract

Rectangular node electrodes were developed with micro-fabrication techniques in order to produce an electrolytic micro-bubbler which, while subjected to a convective flow, can generate bubbles of nearly uniform size with mean diameters of 50 μm or less. The devices were fabricated and placed in both a quiescent tap water chamber and a water channel operating at laminar flow rates. The effect of applied voltage and flow conditions on the bubbles generated was tested on single electrode pairs. Videos of the bubbles generated by the devices were taken from which the bubble sizes and generation rates were recorded.

It was found that higher applied voltages coincided with smaller average bubble size, a narrower distribution of bubble sizes, higher bubble fluxes, and a higher current efficiency. The imposition of a hydrodynamic flow was shown to reduce average bubble size, narrow the range of bubble sizes, and reduce current efficiency. Smaller electrode nodes were seen to reduce the number of active nucleation sites and thus produced a narrower bubble size distribution. In the best case, the bubble distribution was nearly mono-disperse with a small average bubble diameter (ca. 40 μm) with repeatable mean bubble diameters and bubble fluxes. Intermediate values of the ratio of electrode node width and cathode/anode spacing provided the largest average bubble diameters.

Keywords: Bubble; Generation; Electrolysis; Micro-fabrication; Electrode

* Corresponding author. Tel.: +1 217 244 5581.
E-mail address: loth@uiuc.edu (E. Loth).

0301-9322/$ - see front matter © 2005 Elsevier Ltd. All rights reserved.
doi:10.1016/j.ijmultiphaseflow.2005.02.002

1. Introduction

1.1. Motivation for micro-bubble generators

Over the past several decades, methods for reducing skin friction drag have been the subject of intense research. In particular, substantial research has shown that skin friction on flat plates or simple objects can be reduced significantly (e.g. by up to 80%) by injection of micro-bubbles (Merkle and Deutsch, 1992). Although the exact mechanism of micro-bubble drag reduction is not known, studies have indicated that the most effective drag-reducing bubbles are very small, specifically diameters of 50 μm or less (Pal et al., 1988; Duetch, 1999; Kawamura et al., 2003). However, conventional bubblers which use porous plates and compressed gas typically produce bubble diameters 200–800 μm on average with a wide range of sizes due to break-up such that a significant portion of the bubbles may be too big for optimum conditions. The presence of such bubbles in shear flows is consistent with recent detailed measurements by Duhar and Colin (2004). Thus it would be ideal to create a generator which can produce small bubbles that are reasonably mono-disperse, using reproducible micro-fabrication techniques (Lee et al., 2003). In addition, other technologies could benefit from such chemical processes where a large number of small oxygen bubbles are helpful for efficient processing.

Herein, we turn to electrolysis for the bubble generation as it has been shown to generate smaller bubbles. Furthermore, it allows convenience with MEMS-based fabrication which may in turn allow direct control of bubble size, release location, and release frequency. However, it should be cautioned that while such devices may be practical for laboratory scale studies, they may be impractical for large-scale implementation due to aspects of cost, fragility, energy efficiency, etc. In this study, we will examine the capability to produce a continuous stream of small mono-disperse bubbles with micro-fabrication techniques for quiescent and low-flow conditions. However, much more development would be needed before such a device would be practical for laboratory experiments which require bubbly flow clouds, let alone large-scale applications.

1.2. Electrolytic micro-bubble generation

Certain characteristics of electrochemically-generated gas make it amenable for use as a source of micro-bubbles. In fact, the first drag reduction experiments employed fine electrolytic wires wrapped around a body (McCormick and Bhattacharya, 1973). Unlike conventional porous plate bubblers, electrolytic bubble generation does not require a large system of lines and pumps and compared to thermal bubble generation, electrolysis is more energy efficient (Papavasiliou, 2001). Also, previous studies have shown that electrolysis can generate smaller bubbles than conventional porous plates. For instance, in even the distributions containing the largest electrolytically-generated bubbles, Landolt et al. (1970) reported that most diameters were still less than 300 μm. In addition, some studies on electrochemically-generated bubbles (Janssen et al., 1984), have shown a decrease in bubble size with an increase in applied current (and subsequently an increased gas production). This is in contrast to porous plate generation where an increase in gas production is often associated with an increase in bubble size.

A larger, polydisperse bubble population, however, is also consistent with the electrochemical bubble generation size populations measured by Landolt et al. (1970). Micro-fabricated electrodes may be better suited to creating small, mono-disperse populations of bubbles. Studies by Glas and Westwater (1964) and Janssen and Hoogland (1973) indicated an increase in reproducibility with small, polished electrodes, possibly because the small size of the electrodes reduced the number of active nucleation sites.

1.3. Micro-fabricated micro-bubblers

Conceptually, it would be ideal to use reproducible modern micro-fabrication techniques (e.g. used for MEMS devices) to create bubble generators which can produce small bubbles that are reasonably mono-disperse when operated in a flowing water environment. If successfully developed (as is the objective herein), such devices may be formed into matrices to create bubble clouds (which may then allow a substantial reduction in the required gas flux for drag reduction by digitally injecting bubbles with optimum size). The micro-fabrication process can create small electrodes and generates surfaces that are extremely smooth, flat, and clean and hence may produce a more mono-disperse population of bubbles. For instance, previous micro-fabricated devices with artificial nucleation sites have been able to create a mono-disperse population of bubbles (Volanschi et al., 1996). Similar technologies have been used for micro-boiling. Micro-fabricated devices which produced small bubbles (ca. 40 μm) were recently developed for use in pumping devices (Choi et al., 1999), but these micro-bubblers only produced a few bubbles in a quiescent condition.

2. Methodology

2.1. Quiescent and water channel facilities

Tests under quiescent conditions were conducted at room temperature and atmospheric pressure under a microscope in a chamber filled with tap water for quiescent conditions. For this setup, four pieces of thin Plexiglas were attached to the micro-bubbler with epoxy to form a tank to hold water directly on top of the exposed electrode nodes. The micro-bubbler was then vacuum-mounted under the microscope. Lighting was provided by a fiber optic illuminator with flexible light guides and a constant voltage was applied to the electrode contacts using a DC voltage source and probes. The setup is shown in Fig. 1a.

To test the bubble generation under a test flow, a small-scale water channel was designed and constructed. The channel (Fig. 1b) had a total capacity of approximately 2.5 l of tap water and a recirculation length of approximately 3.6 m. A small honeycomb section (with an inner cell diameter of approximately 1/6 the channel height) was placed in the entrance of the test section to straighten the flow. The 19 mm square test section was situated horizontally and was approximately 1 m long. It provided optical access on all sides through four Plexiglas walls, which were approximately 13 mm thick. The test section was comprised of three sections, including a flow

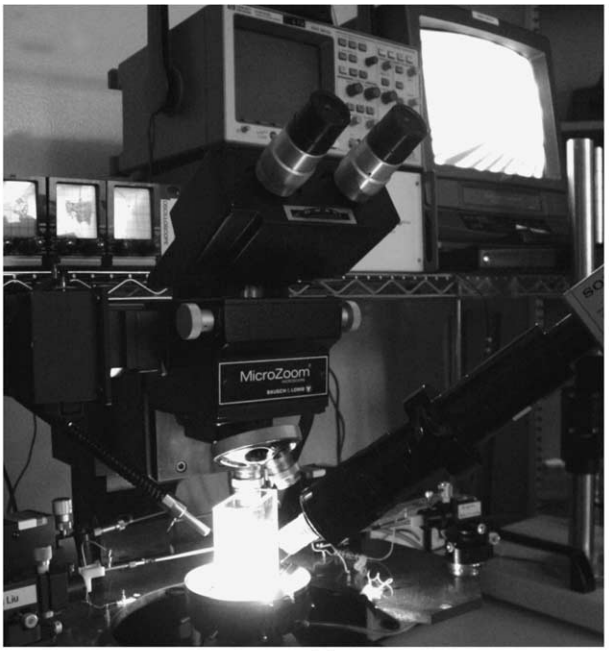

(a)

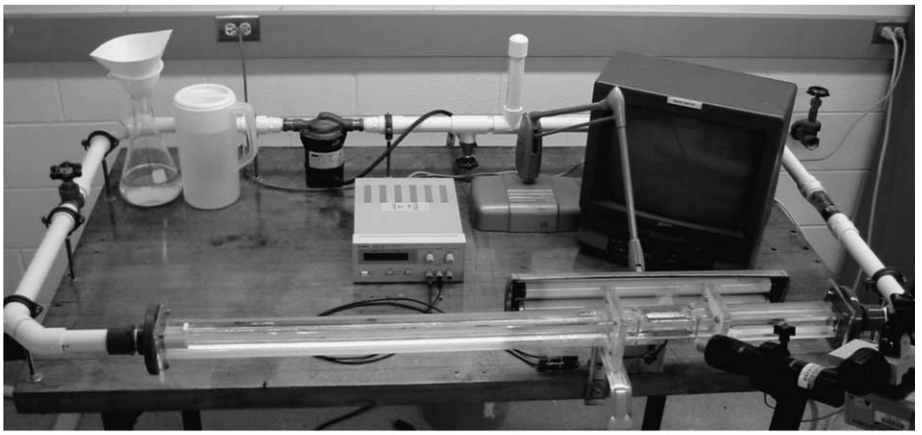

(b)

Fig. 1. Photograph of micro-bubblers in (a) quiescent tank, (b) water channel.

development section which was approximately 32 times the effective channel height, long enough for fully developed laminar flow.

The test section also included a removable micro-bubbler section that had a detachable wall on which the micro-bubblers were mounted. The micro-bubbler was flush mounted on the detachable wall of the water channel such that only the electrode nodes were exposed to water and the electrode contacts were accessible outside of the channel. The micro-bubbler was used in the ''plate on bottom'' configuration so that the buoyancy force would facilitate the removal of the bubbles

from the injector. To rid the channel of any trapped residual air, the water was allowed to circulate for an hour before the beginning of any experiments. The water flow rate was controlled by a gate valve located before the test section and was measured using a spring-loaded variable area flow-meter (with an accuracy of 2%) situated after the test section. Voltage was applied to the cathode and anode of an electrode pair using an HP power supply and retractable hook test leads. The applied voltage and current were measured using a Fluke multi-meter.

To keep operating conditions consistent, the same water supply was used for the experiments. Before the start of the experiments, the water supply was allowed to sit for at least two days to de-gas. The temperature and the pH of the water were taken before, during, and after the experiments with little variation observed. The average recorded temperature was 29 °C and the average pH was 7.2.

2.2. Bubble sizing

For quantitative bubble sizing, a Sony CCD (1/2″ CCD) color video camera equipped with an Infinivar CFM microscope video lens was used with an articulating arm boom stand, a fluorescent lamp, frosted paper, and a computer/video capture card. The fluorescent lamp and frosted paper were placed in front of the camera to provide diffused backlighting, minimizing reflections and creating high contrast images with clearly defined bubble edges (Hugi and Mueller, 1993), allowing the diameters to be measured. During the experiments, video of the micro-bubbler in operation was taken. Individual frames of bubbles immediately after detachment were exported from the digital video. These images were then imported into Photoshop and the bubble diameter measured in pixels was compared to the reference image length also measured in pixels (usually an electrode whose actual width was verified under a microscope), allowing measurement of the diameters and the moments of bubble release. From this, average bubble diameters and generation rates could be determined. The mean bubble diameter at each test condition was determined based on an ensemble average. The bubble measurement technique was calibrated by measuring silica micro-spheres of known diameter. The measurement was within 6% for an approximately 90 μm sphere and within 5% for an approximately 140 μm sphere. The bubble measurement technique was further calibrated in a quiescent flow using measurements of terminal velocity compared to expected values. The expected terminal velocity was based on a drag coefficient C_D of $48/Re_p$ which is reasonable for bubbles in contaminated water since $Re_p \ll 1$, where Re_p is the bubble Reynolds number based on terminal velocity and bubble diameter (Loth, 2000; Felton and Loth, 2001). The resulting uncertainty in average bubble diameter, based on a comparison of results from the two techniques, was estimated to be 4 μm or less for bubble diameters ranging from 30 to 60 μm.

2.3. Fabrication and micro-bubbler design

The fabrication process (Fig. 2) for the micro-bubblers starts with a piece of silicon or glass substrate. First, thermal evaporation is used to grow a 200-Å thick film of chrome followed by a 2000-Å thick film of gold, as shown in Fig. 2a. The chrome is deposited first to serve as an adhesion prompter for the gold electrode layer. The Cr/Au film is then patterned, using photo-lithography (using a Karl Suss Mask Aligner) and wet etching of the metal, to form the electrodes and

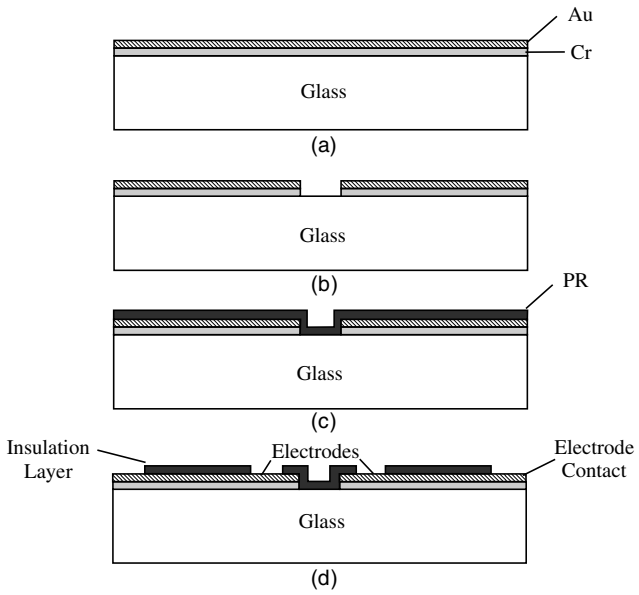

Fig. 2. Micro-bubbler fabrication process; note that coating thicknesses are exaggerated (not to scale).

the electrode contacts (Fig. 2b). Next, a 1.5-μm thick layer of photo-resist (PR) is spun on (Fig. 2c) to serve as an insulating dielectric layer. Alternatively, the insulation layer can be formed out of photo-definable polyimide or Parylene. The photo-resist layer is then patterned with photolithography, leaving only the desired electrode nodes and their contacts exposed (Fig. 2d). Finally, a bake-out is performed; further details are available in Lee (2003).

A schematic of the overall design is shown in Fig. 3a, where a voltage could be applied over various Cr/Au contact leads to activate a single node pair (a cathode and an anode). Note that the coating thicknesses are small (less than 2 μm) such that the surface is hydraulically smooth. The node pair design employed rectangular exposed surfaces, characterized by a node width (w), length (l), and spacing (s) as shown in Fig. 3b. The first-generation device was fabricated to test the effect of applied voltage (up to 4.1 V) on bubble generation with electrodes of constant geometry. The exposed electrodes were rectangular, with $w \sim 100$ μm, $l \sim 125$ μm, and $s \sim 400$ μm. A micro-graph showing a close-up of the array is given in Fig. 4a. The micro-bubbler was operated in both a quiescent condition ($Re = 0$) and under a laminar flow ($Re = 370$), where Re is based on the channel effective diameter and the flow condition of 1.75 cm/s.

The second-generation device, in which the electrode area and the spacing between the electrodes were reduced and varied (Fig. 4b), was fabricated and tested at constant voltage in quiescent conditions to determine the effect of the electrode geometry on bubble generation. This micro-bubbler included smaller, compared to the previous device, square electrodes ($w = l$) with dimensions ranging from 40 μm to 100 μm. The smaller size was intended to reduce the number of nucleation sites and thus increase the uniformity of the generated bubbles. The space between the anode and cathode (s) was also reduced, ranging from 80 μm to 200 μm, in an attempt to decrease the resistance between the electrode pair and thus decreasing the voltage needed to generate

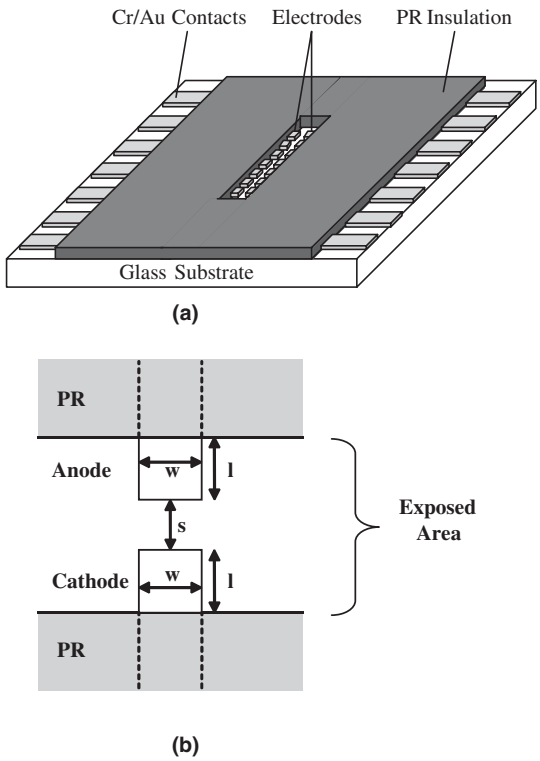

Fig. 3. Schematic of micro-bubbler. (a) Overall view (note that coating thickness of nodes and PR coating is exaggerated). (b) Definition of exposed node geometry dimensions where flow direction (when present) will be left to right.

bubbles. Tests were conducted under quiescent conditions with a constant applied voltage of 3.7 V. In general, the electrolysis could go for tens of minutes with no polarization noted.

3. Results

3.1. First-generation micro-bubbler (applied voltage, average flow velocity)

The physics of the bubble generation and release were first studied in the quiescent flow facility. Then, to understand the response to fluid motion, the micro-bubbler was transferred to the water channel facility. The production of bubbles with the first-generation micro-bubbler was generally successful. It was observed that the threshold voltage (the minimum voltage required to generate a noticeable bubble) was approximately 3.2 V regardless of the flow conditions. This is significantly greater than the decomposition potential, 1.2 V, and higher than the over-potentials measured in Glas and Westwater (1964), indicating that fairly high levels of supersaturated gas were required for nucleation on this device. In addition, the maximum voltage that could be applied was approximately 6 V, as some deterioration of the electrodes and cracking of the PR insulation layer began

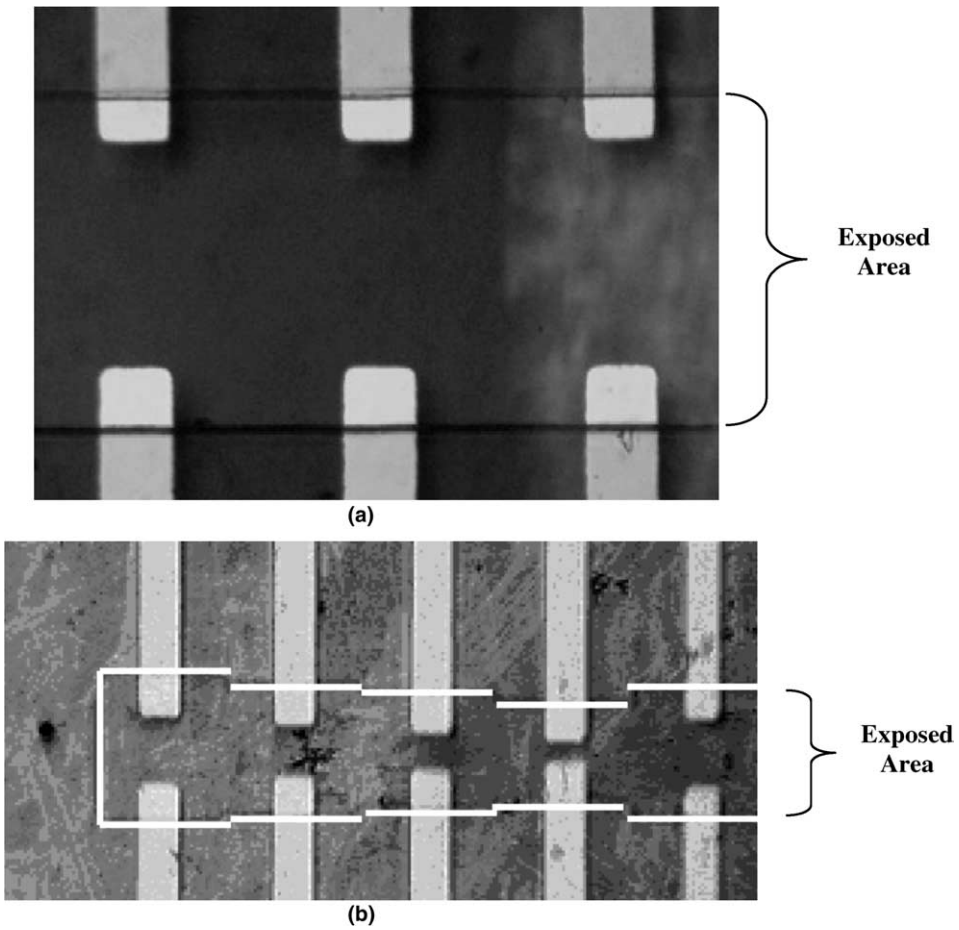

Fig. 4. Micro-graphs of fabricated node geometries where flow direction (when present) will be left to right: (a) first-generation devices, (b) second-generation devices.

to appear at this voltage level. In general, the current across the entire device was relatively small and nearly constant in all cases, increasing linearly with applied voltage. The measured current varied from 0.05–0.11 mA for the range of voltages tested. Expected fluctuations in current as the bubble covering the electrode surface grew were not observed, probably due to the comparatively large electrode surface and the fact that the bubbles tended to nucleate on the edges resulting in a low fractional surface coverage of the electrode node.

For each bubble generated, heterogeneous nucleation, i.e. nucleation at an interface between the liquid and the electrode, was observed. This is expected as the nucleation energy barrier for homogeneous nucleation is expected to be significantly greater. There seemed to be a higher density of active nucleation sites at the interface between the water and the edges of the electrodes, where surface imperfections were probably introduced on the electrodes during the wet-etching used to define their shape. An image of micro-bubbles releasing from three active nucleation sites is given in Fig. 5a. In general, the bubble would not instantly detach when formed. Instead, it

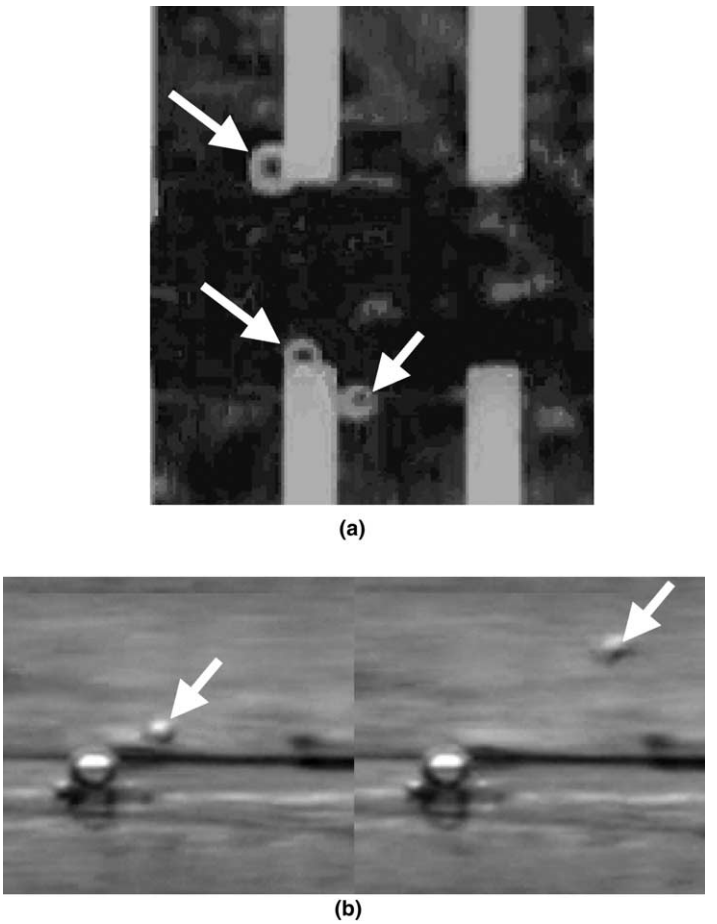

Fig. 5. Bubbles releasing from first-generation device subjected to a flow rate: (a) from above, showing three bubbles (see arrows) which are growing, and (b) from the side, showing two sequential images of a bubble just before and just after release (see arrows).

would continue to grow until its size was large enough such that buoyancy, convective, and electrostatic forces could pull it off. Images of a sequence of bubble growth and detachment subjected to a flow are given in Fig. 5b, where the bubble is seen just before release and then just after, where it follows a trajectory imposed by the flow and buoyancy. When subjected to a flow, observed incidents of coalescence were more infrequent. This can be attributed to the increased spacing of any bubble pairs as they are accelerated away from the wall as well as the flow providing resistance against the movement of neighboring bubbles towards each other.

To observe the generation sensitivity to variation in the electric input, the mean diameter of the bubbles was measured as a function of voltage (Fig. 6). It was seen that the average bubble departure diameter decreased as the voltage was increased. This is in qualitative agreement with the trends noted in Janssen et al. (1984) and Vogt (1989) for larger electrodes (ca. 3 cm^2). Note that this trend is not consistent with the findings of Chin et al. (1988) and Landolt et al. (1970), for wires and flat electrodes. As the applied voltage was increased, it was observed that active

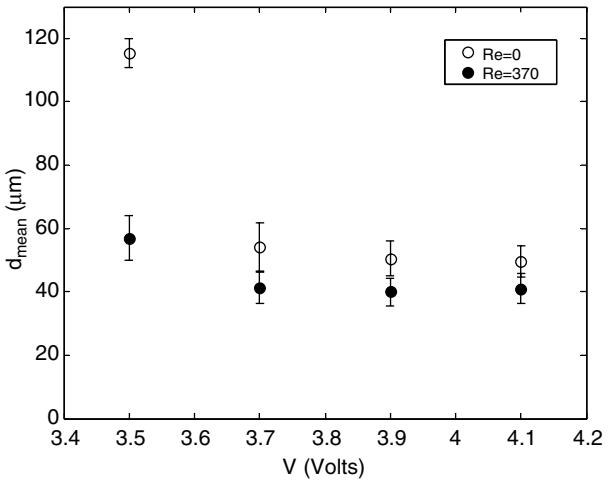

Fig. 6. Mean bubble size sensitivity to voltage for first-generation bubblers for no-flow and laminar-flow conditions showing 95% confidence levels.

nucleation sites tended to increase in number with smaller bubbles generated from the additional sites, which may be a reason for the smaller mean diameter.

The voltage changes can have a potential impact on the bubble charge, which could also explain the observed smaller diameters as voltage increased. Brandon and Kelsall (1985) noted that electrochemically generated bubbles generally acquire a negative charge for a pH greater than 3 (as is herein) with the magnitude of the charge increasing with increasing current density. Nefedov et al. (1999) believed this was due to the accumulation of ions near the bubble surfaces because of the loss of electroneutrality in the solution layer that surrounds the bubble. As the applied voltage increased for the present tests, so did the current (and subsequently the current density) and hence the negative charge of the electrochemically-generated bubbles should increase as well. The negatively charged H_2 bubbles would then be repelled at the cathode while the negatively charged O_2 bubbles would be attracted at the anode. The number of H_2 bubbles generated, however, should be greater than the number of O_2 bubbles generated since twice as much H_2 gas is theoretically produced by the electrolysis of water, H_2 current efficiency is greater (Chin et al., 1988), and H_2 bubbles have a weaker adhesion force (Chin et al., 1988) for the same applied current. The net effect should be a lowering of the mean diameter as the voltage, and hence the negative charge of the bubbles, is increased because the repulsive effect on H_2 bubbles should outweigh the effect of the attractive forces on the O_2 bubbles due to their greater numbers.

Also, micro-convection, convection caused by the expanding bubble diameter of neighboring bubbles (Vogt, 1978), should increase as the applied voltage increases due to an increase in the bubble growth rate and the number of nucleation sites and adhering bubbles (average population density). This increased micro-convection would tend to promote the detachment of neighboring bubbles. The addition of a drag side-force on the bubble just before detachment explains the reduction of the bubble size for flow conditions, similar to the trend observed by Thorncroft et al. (1988) whereby boiling bubble diameters decreased consistently as convection speeds increased. As the voltage increased, the difference between the average bubble departure diameters

at $Re = 0$ and $Re = 370$ was seen to decrease. This may be explained by the subsequent increase in the influence of micro-convection and electrostatic forces as the mechanism of bubble detachment as the number of active nucleation sites and the charge acquired by the bubbles increases with voltage.

While this first-generation device created a significant portion of small bubbles, the resulting bubble size distribution was not as mono-disperse as desired, as seen qualitatively in Fig. 7. The lack of uniformity in bubble size may be attributed to the presence of multiple active nucleation sites, such that bubbles from one site tended to vary in size from others created at the other sites, and the coalescence of bubbles generated from nucleation sites in close proximity. Further limiting the area of the electrodes, and thus possibly limiting nucleation to a single site, could lead to more uniform bubble sizes (Glas and Westwater, 1964). From the bubble diameter distributions, it is noticed that as the voltage is increased, instances of larger bubbles were reduced, in contrast to the results of Landolt et al. (1970).

The average rate of bubble generation was also observed to increase as the applied voltage was increased (Fig. 8a), in qualitative agreement with the work of Chin et al. (1988). This was also expected as Faraday's Law of Electrolysis states that the amount of a gas liberated by electrolysis

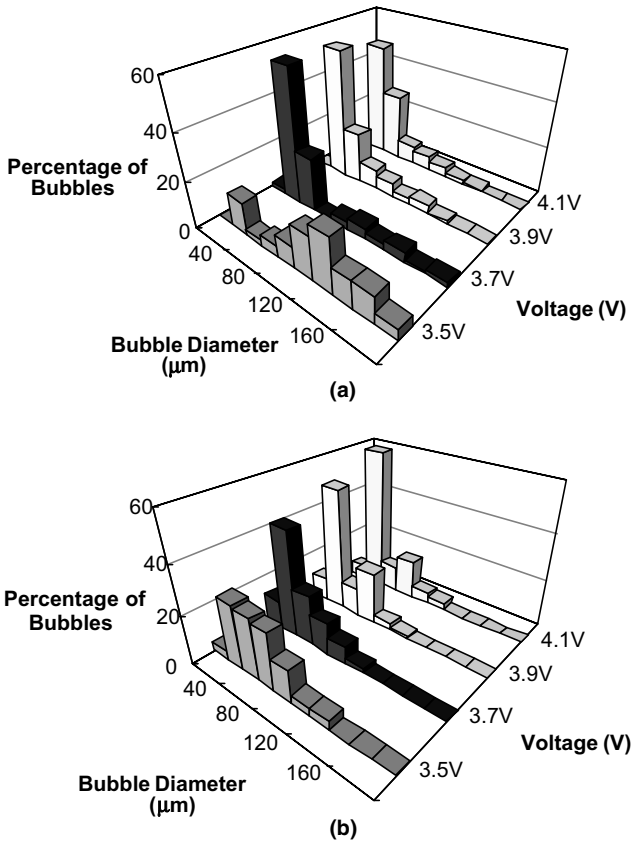

Fig. 7. Size distribution for first-generation micro-bubblers with 20 μm bin widths: (a) quiescent conditions ($Re = 0$), and (b) water channel flow conditions ($Re = 370$).

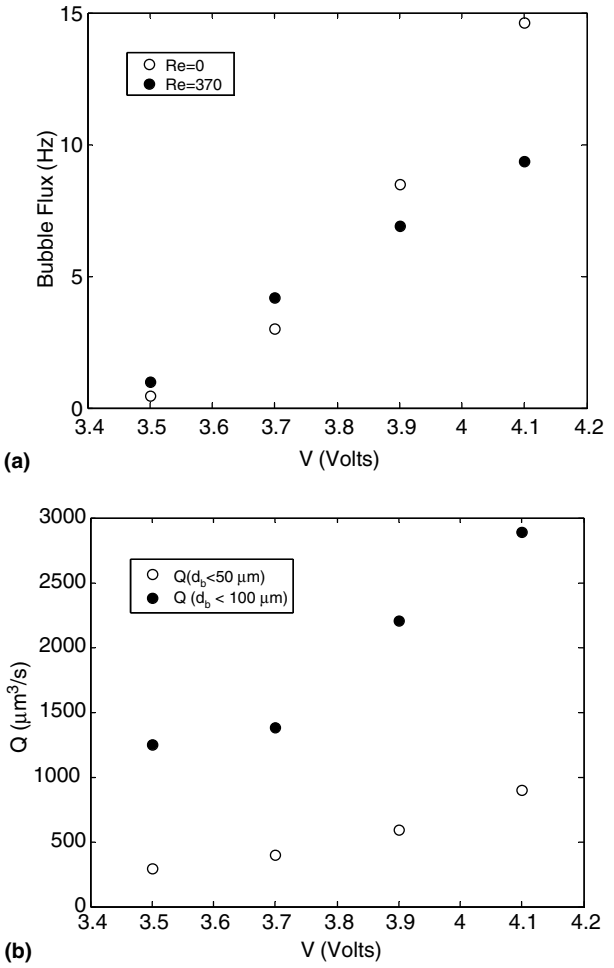

Fig. 8. The effect of voltage for the first-generation on (a) average bubble number flux, and (b) average bubble volumetric flux at $Re = 370$.

is linearly proportional to the current applied. With a decrease in average bubble size with increasing voltage, the rate at which bubbles are generated must increase if the volumetric flux is to increase. Also, it should be expected that the addition of a hydraulic drag force promoting detachment of bubbles should increase the bubble detachment frequency, as seen in Chin et al. (1988). This trend, however, was only seen here at the lower voltages.

The amount of gas consisting of small bubbles was seen to increase under quiescent and low Reynolds number flow (Fig. 8b for $Re = 370$) as the applied voltage was increased. This indicates that at the higher voltages, not only does the rate of gas generation increase, but the efficiency of generating gas comprised of bubbles with smaller diameters also increases. This is in stark contrast to the reported bubble diameter/gas injection rate relationship for a porous plate where an increase in the gas injection rate will lead to an increase in bubble sizes and thus a reduction in the efficiency in creating small bubbles (Pal et al., 1988).

The current efficiency, the ratio of the actual gas generated to the theoretical gas generated if all the produced gas comes out of the solution as a bubble, was seen to increase with an increase in voltage and seen to decrease in the presence of a flow velocity. Both trends were also reported by Chin et al. (1988). The decrease in current efficiency in the presence of a flow is expected as the increased flow may remove dissolved gas from the near electrode area, thus reducing the local supersaturation concentration.

3.2. Second-generation results (node diameter/spacing)

A second-generation micro-bubbler was fabricated in which the width of the square electrodes and the distance between the cathodes and anodes were reduced from the first-generation device and varied. By changing the electrode geometry, it was observed that the minimum voltage necessary to generate bubbles decreased, the minimum threshold voltage being approximately 2.7 V (versus 3.2 V for the first-generation device) indicating that bringing the electrodes closer together and reducing the size may lead to an increased local supersaturation concentration near potential nucleation sites. Two sets of geometries were tested (where $w = l$ in all cases): (1) width of the electrodes (w) was held constant and the spacing between the anode and cathode (s) was varied; and (2) spacing was held constant and electrode width was varied. The bubble size distributions for

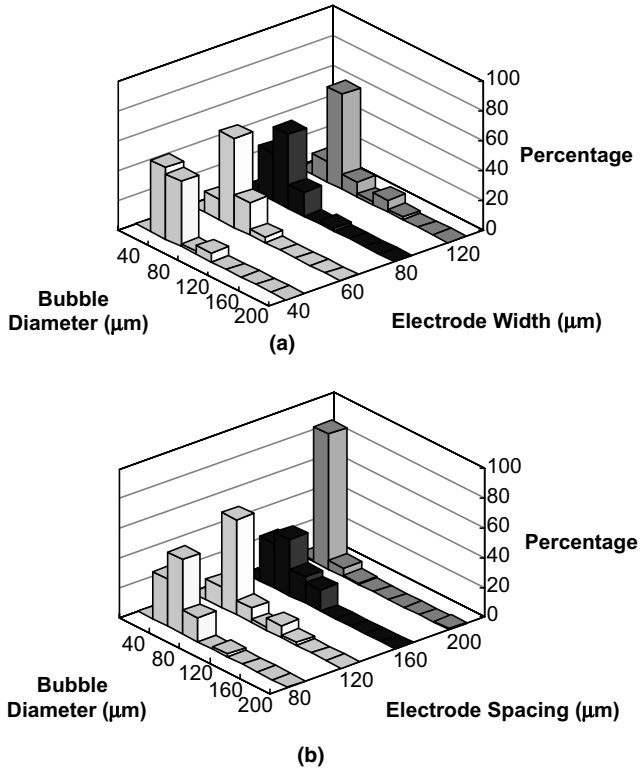

Fig. 9. Size distribution for second-generation micro-bubblers with 20 μm bin widths: (a) variation in electrode width, and (b) variation in electrode spacing.

these two parametric studies are given in Fig. 9 and it is observed qualitatively that the size distribution of generated bubbles narrowed compared to the first-generation device, nearly all the bubbles were below 100 μm in diameter. This is most likely due to the reduced electrode area and thus the reduction in the number of nucleation sites. In the best case, $w = 80$ μm and $s = 200$ μm, nearly all bubbles nucleated from the same site and 90% of the bubbles were within 20 μm of the mean diameter.

Interestingly, the average bubble size did not monotonically decrease or increase as a function of spacing and width, and the trends tended to be observed for similar values of width to spacing ratio. To explore this further, the mean diameter examined from Fig. 9 was plotted as a function of w/s in Fig. 10a. The mean bubble diameter seems to peak at intermediate values of the ratio between electrode size and spacing, specifically for a w/s of about 0.7. One explanation for this

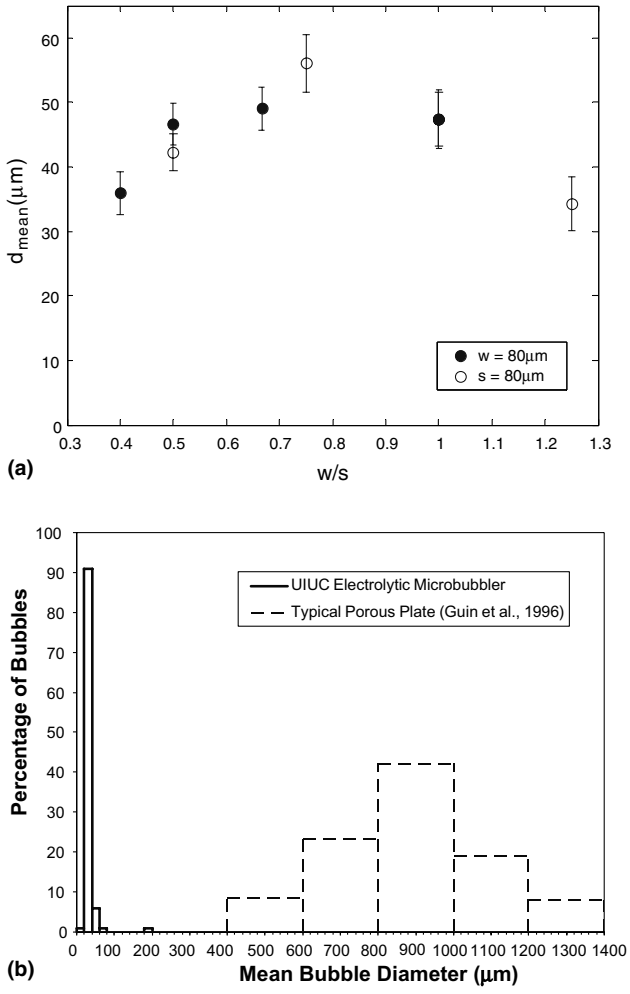

Fig. 10. Second-generation micro-bubbler results: (a) effect of the width/spacing ratio on mean diameter with 95% confidence intervals, and (b) comparison of narrowest bubble distribution and an estimated porous plate distribution.

is a decrease in bubble coalescence when the dimensionless electrode area is too small or too big. When the dimensionless electrode size is largest (w/s is greatest), multiple nucleation sites are farther apart from each other as bubbles tend to form on the edges of the electrode and incidences of bubble coalescence are reduced. When dimensionless electrode size is smallest (w/s is smallest), coalescence may be reduced due to the reduction in nucleation sites. It may be that at the intermediate values of the w/s ratio, multiple nucleation sites exist in relatively close proximity, leading to more incidences of coalescence. This relationship between the size and spacing ratio is not well understood; further research is suggested to determine its effects.

In general, manipulation of the size and spacing of the electrodes affected the bubble size distributions, probably by changing the number of nucleation sites. In the $w = 80\ \mu m/s = 200\ \mu m$ configuration, the bubbles nucleated almost exclusively from one site and the mean bubble diameter was smallest. The size distribution from this configuration is compared against the estimated bubble distribution from a conventional porous plate (Guin et al., 1996) in Fig. 10b. The result demonstrates the ability of the micro-bubbler to create smaller bubbles in a narrower range of sizes than those from a porous plate (also note that the porous plate was operated at much higher flow velocities which would probably further reduce the electrolytic bubble sizes). Three separate runs from this particular electrode geometry were recorded and data taken. It was observed that when averaged, both the average bubble diameter and the average bubble flux were fairly repeatable, indicating the importance of limiting nucleation to one site to improve reproducibility.

4. Summary

Several micro-fabricated electrolytic micro-bubblers were fabricated and tested under a microscope and in a square water channel under quiescent and fully developed laminar flow conditions. The fabricated micro-bubblers were capable of creating significant numbers of small bubbles. In particular, at the higher voltages, the first-generation device was able to generate over 65% of its bubbles under a diameter of 50 μm for both quiescent and low-flow conditions. The mean diameters of the detached bubbles for the first-generation micro-bubblers decreased as the applied voltage was increased. Furthermore, as the flow velocity was increased, the average departure diameter also decreased, which may be explained by the flow tearing the bubbles from the surface (even at the low speed of 1.7 cm/s) as well as a reduction in coalescence events. The difference between the average bubble diameter in the presence and in the absence of a hydrodynamic flow was seen to decrease as the applied voltage was increased, possibly due to the increased influence of micro-convection and electrostatic repulsion in the detachment of bubbles.

The average rate of bubble generation increased as the applied voltage (and thus current) was increased, consistent with Faraday's Law of Electrolysis. The amount of gas consisting of small bubbles was seen to increase under quiescent and low Reynolds number flow as the applied voltage was increased. The current efficiency was also seen to increase with an increase in voltage but decreased in the presence of a flow velocity. A decrease in average bubble size from the first to second generation was seen as the electrode size was reduced. It was noted that the mean bubble diameter tended to decrease when the ratio between the electrode size and electrode distance was much more or much less than a ratio of 0.7. In the optimum case, nucleation was limited to one site and better than 90% of the generated bubbles were within 20 μm. In this case, the bubble

distribution was nearly mono-disperse and average bubble diameter and bubble flux were fairly repeatable over repeated runs. However, much more development would be needed before such a device would be practical even for simple small-scale laboratory experiments which require bubbly flow clouds. In particular, quantification and optimization of gas generation efficiency and the testing in liquids with a wider (and more precisely documented) range of conditions is needed.

Acknowledgment

This work was also supported by the Defense Advanced Research Projects Agency (DARPA) under grant MDA972-01-C-0042 with Dr. Lisa Porter as technical monitor.

References

Brandon, N.P., Kelsall, G.H., 1985. Growth kinetics of bubbles electrogenerated at microelectrodes. J. Appl. Electrochem. 15, 475–484.

Chin, J.M., Janssen, L.J.J., van Stralen, S.J.D., Verbunt, J.H.G., Sluyter, W.M., 1988. Bubble parameters and efficiency of gas bubble evolution for a chlorine-, a hydrogen-, and an oxygen-evolving wire electrode. Electrochim. Acta 33, 769–779.

Choi, B.K., Ma, M., White, C., Liu, C., 1999. Electrolytic and thermal bubble generation using AC inductive powering. In: International Conference on Solid-State Sensors and Actuators, Transducer'99, Sendai, Japan.

Duhar, G., Colin, C., 2004. A predictive model for the detachment of bubbles injected in a viscous shear flow with small inertia effects. Phys. Fluids 16, L31–L34.

Duetch, S., 1999. Combined Microbubble and Polymer Drag Reduction, A Review. ONR Workshop on Gas-Based Surface Ship Drag Reduction, 7–8 October, Newport, RI.

Felton, K., Loth, E., 2001. Spherical bubble motion in a turbulent boundary layer. Phys. of Fluids 13, 2564–2577.

Glas, J.P., Westwater, J.W., 1964. Measurements of the growth of electrolytic bubbles. Int. J. Heat Mass Transfer 7, 1427–1443.

Guin, M.M., Kato, H., Yamaguchi, H., Miyanaga, M., Maeda, M., 1996. Direct skin friction measurements and observation of drag reduction in a two-phase air–water channel. In: 1996 Fluids Engineering Division Conference, FED vol. 237, pp. 93–100.

Hugi, C., Mueller, A., 1993. A camera for measuring density, size and velocity of rising air bubbles and water velocity in a bubble plume. In: Flow Visualization and Image Analysis. Kluwer Academic Publishers, Dordrecht, pp. 189–205.

Janssen, L.J.J., Hoogland, J.G., 1973. The Effect of electrolytically evolved gas bubbles on the thickness of the diffusion layer-II. Electrochim. Acta 18, 543–550.

Janssen, L.J.J., Sillen, C.W.M.P., Barendrecht, E., van Stralen, S.J.D., 1984. Bubble behaviour during oxygen and hydrogen evolution at transparent electrodes in KOH solution. Electrochim. Acta 29, 633–642.

Kawamura, T., Moriguchi, Y., Kato, H., Kakugawa, A., Kodama, Y., 2003. Effect of bubble size on the microbubble drag reduction of a turbulent boundary layer. In: 4th ASME–JSME Joint Fluids Engineering Conference, Honolulu, HI, July 6–10, 2003.

Landolt, D., Acosta, R., Muller, R.H., Tobias, C.W., 1970. An optical study of cathodic hydrogen evolution in high-rate electrolysis. J. Electrochem. Soc. 117, 839–845.

Lee, S., 2003. Electrolytic Microbubble Injection in a Water Channel. M.S. Thesis. Department of Mechanical Engineering, University of Illinois at Urbana-Champaign, IL.

Lee, S., Sutomo, W., Liu, C., Loth, E., 2003. MEMS-based electrolytic microbubbler in a water channel. In: 4th ASME/JSME Fluids Engineering Conference, Honolulu HA, July, FEDSM2003-45646.

Loth, E., 2000. Numerical approaches to dilute two-phase flow. Prog. Energy Combustion Sci. 26, 161–223.
McCormick, M.E., Bhattacharya, R., 1973. Drag reduction of a submersible hull by electrolysis. Naval Eng. J. 85, 11–16.
Merkle, C., Deutsch, S., 1992. Microbubble drag deduction in liquid turbulent boundary layers. Applied Mechanics Reviews 45, Part1, March, ASME Book No. AMR 105.
Nefedov, V.G., Naslednikov, A.V., Serebritskii, V.M., 1999. Electrical properties of electrolytically generated gas bubbles. Colloid J. 61, 342–347.
Pal, S., Merkle, C.L., Deutsch, S., 1988. Bubble characteristics in a microbubble boundary layer. Phys. Fluids 31, 751–774.
Papavasiliou, P.P., 2001. Bubble-Actuated Planar Microvalves. Ph.D. Thesis. University of California, Berkeley.
Thorncroft, G.E, Klausner, J.F., Mei, R., 1988. An experimental investigation of bubble growth and detachment in vertical upflow and downflow boiling. Int. J. Heat Mass Transfer 41, 3857–3871.
Vogt, H., 1978. Mass transfer at gas evolving electrodes with superposition of hydrodynamic flow. Electrochim. Acta 23, 203–205.
Vogt, H., 1989. The problem of the departure diameter of bubbles at gas-evolving electrodes. Electrochim. Acta 34, 1429–1432.
Volanschi, A., Oudejans, D., Olthuis, W., Bergveld, P., 1996. Gas phase nucleation core electrodes for the electrolytical method of measuring the dynamic surface tension in aqueous solutions. Sensor. Actuator. B 35–36, 73–79.